

Depletion “skraps” and dynamic buffering inside the cellular calcium store

Bradley S. Launikonis*, Jingsong Zhou*, Leandro Royer*, Thomas R. Shannon*, Gustavo Brum†, and Eduardo Ríos**

*Section of Cellular Signaling, Department of Molecular Biophysics and Physiology, Rush University, 1750 West Harrison Street, Suite 1279JS, Chicago, IL 60612; and †Departamento de Biofísica, Universidad de la República, Facultad de Medicina, Montevideo, Uruguay

Communicated by Clara Franzini-Armstrong, University of Pennsylvania School of Medicine, Philadelphia, PA, December 28, 2005 (received for review November 29, 2005)

Ca²⁺ signals, produced by Ca²⁺ release from cellular stores, switch metabolic responses inside cells. In muscle, Ca²⁺ sparks locally exhibit the rapid start and termination of the cell-wide signal. By imaging Ca²⁺ inside the store using shifted excitation and emission ratioing of fluorescence, a surprising observation was made: Depletion during sparks or voltage-induced cell-wide release occurs too late, continuing to progress even after the Ca²⁺ release channels have closed. This finding indicates that Ca²⁺ is released from a “proximate” compartment functionally in between store lumen and cytosol. The presence of a proximate compartment also explains a paradoxical surge in intrastore Ca²⁺, which was recorded upon stimulation of prolonged, cell-wide Ca²⁺ release. An intrastore surge upon induction of Ca²⁺ release was first reported in subcellular store fractions, where its source was traced to the store buffer, calsequestrin. The present results update the evolving concept, largely due to N. Ikemoto and C. Kang, of calsequestrin as a dynamic store. Given the strategic location and reduction of dimensionality of Ca²⁺-adsorbing linear polymers of calsequestrin, they could deliver Ca²⁺ to the open release channels more efficiently than the luminal store solution, thus constituting the proximate compartment. When store depletion becomes widespread, the polymers would collapse to increase store [Ca²⁺] and sustain the concentration gradient that drives release flux.

calcium signaling | calcium sparks | excitation–contraction coupling | sarcoplasmic reticulum | skeletal muscle

Rapid changes in intracellular cytosolic [Ca²⁺] are required for signaling functions in many cell types (1). These changes are achieved via Ca²⁺ release through channels, ryanodine receptors (RyRs), which must open and close quickly. To increase its speed, gating of RyRs relies on effects of the permeant ion, including channel opening by elevated cytosolic [Ca²⁺] (2). In muscle, the desirable fast kinetic features are already present in its elementary signaling events, Ca²⁺ sparks (3), which involve the nearly simultaneous opening (4) of a number of channels (5), followed by their synchronized closing (4). Thus, this gating does not follow the usual Markovian rules for channels that evolve independently but requires time-keeping and synchronization (6). In cardiac muscle, depletion of sarcoplasmic reticulum (SR) Ca²⁺ is the likely timer of channel closing, and the substantial depletion that follows the cardiac beat (7) was imaged as “blinks” associated with Ca²⁺ sparks (8). The sensor that translates depletion into channel closing appears to be the main intra-SR buffer, calsequestrin (CSQ) (9).

By contrast, in skeletal muscle, depletion associated with a twitch is only 8–15% (10). This low rate of depletion reflects a SR with larger terminal cisternae containing higher concentrations of a CSQ of greater binding capacity, thus constituting a much greater calcium reservoir. Despite the greater store, sparks of skeletal muscle are even briefer and more stereotyped than in cardiac muscle, which casts doubts on the signaling role of depletion in skeletal muscle and elsewhere.

To ascertain the magnitude and role of Ca²⁺ depletion, we combined shifted excitation and emission ratioing of fluores-

cence (SEER) imaging of [Ca²⁺] in the SR, [Ca²⁺]_{SR} (11) with confocal imaging of cytosolic [Ca²⁺] in frog skeletal muscle. First we sought images of the depletion associated with sparks, which we named “skraps” *a priori*, expecting mirror images of sparks. We had two surprises: Skraps did not mirror sparks but had their own suggestive kinetics. Also, cell-wide Ca²⁺ release was often accompanied by increases in free intrastore [Ca²⁺].

Results

Simultaneous Imaging of [Ca²⁺] in Cytosol and SR Lumen. The evolution of [Ca²⁺]_{SR} was monitored by the ratio of simultaneously recorded SEER (11) images (F_1 and F_2) of SR-trapped mag-endo-1. Cytosolic [Ca²⁺] was monitored by the fluorescence, F_3 , of rhod-2 placed in the cytosol. Fig. 1*A* is a line-scan image of $F_3(x, t)$ in a frog muscle cell with permeabilized plasmalemma immersed in a sparks-promoting solution. Fig. 1*B* is the ratio $R(x, t)$ of F_1 and F_2 , obtained simultaneously with F_3 . R is a monotonic function of [Ca²⁺]_{SR} calibrated *in situ* (11).

[Ca²⁺] varied between 300 μ M and 1 mM in non-spark regions (10 cells). The circles in Fig. 1*A* were placed by an automatic detector of sparks. Those in Fig. 1*B* mark the corresponding spatiotemporal locations in the R image. No depletion was evident to the eye at these locations. For every spark, the surrounding subarray within the image was extracted (dashed rectangle); their average is in Fig. 1*C* (numbers of cells and events averaged are given in the Table 1). Fig. 1*D* is the corresponding average of R images, with the spark overlapped as a contour. Instead of the expected depression in [Ca²⁺]_{SR}, we found a stable increase of $\approx 5\%$ of the resting value of R , or an increase of $\approx 10\%$ in [Ca²⁺] monitored by the dye.

Skraps of SR Depletion. [Ca²⁺] increases in mitochondria upon Ca²⁺ release (12) and mag-endo-1 loads in mitochondria as well as SR (11). When imaging in cells exposed to four inhibitors of mitochondrial Ca²⁺ uptake (Fig. 1*E* and *F*), the local increase in organellar [Ca²⁺] was greatly reduced, and a small depression was found on the central ridge of increased [Ca²⁺] at the time of the spark. The profiles of the normalized and filtered $R(x, t)$ image are in Fig. 1*G* and *H*. The decay in R (blue trace) started at the same time as the spark (red trace), reaching a nadir, down 0.6% from the starting value after an interval of ≈ 45 ms. The recovery had a time constant of 48 ms.

The skraps were defined better by replacing glutamate with sulfate in the solution, which widens sparks (as shown in Fig. 2*A*) probably by recruitment of channels (13). The local increase in organellar [Ca²⁺] was not found in sulfate, irrespective of the presence of mitochondrial inhibitors (Table 1). This effect of sulfate supports a mitochondrial origin of the increase, because sulfate is not a substrate for mitochondrial metabolism. Fig. 2*B*

Conflict of interest statement: No conflicts declared.

Abbreviations: RyR, ryanodine receptor; SR, sarcoplasmic reticulum; CSQ, calsequestrin; SEER, shifted excitation and emission ratioing of fluorescence.

†To whom correspondence should be addressed. E-mail: erios@rush.edu.

© 2006 by The National Academy of Sciences of the USA

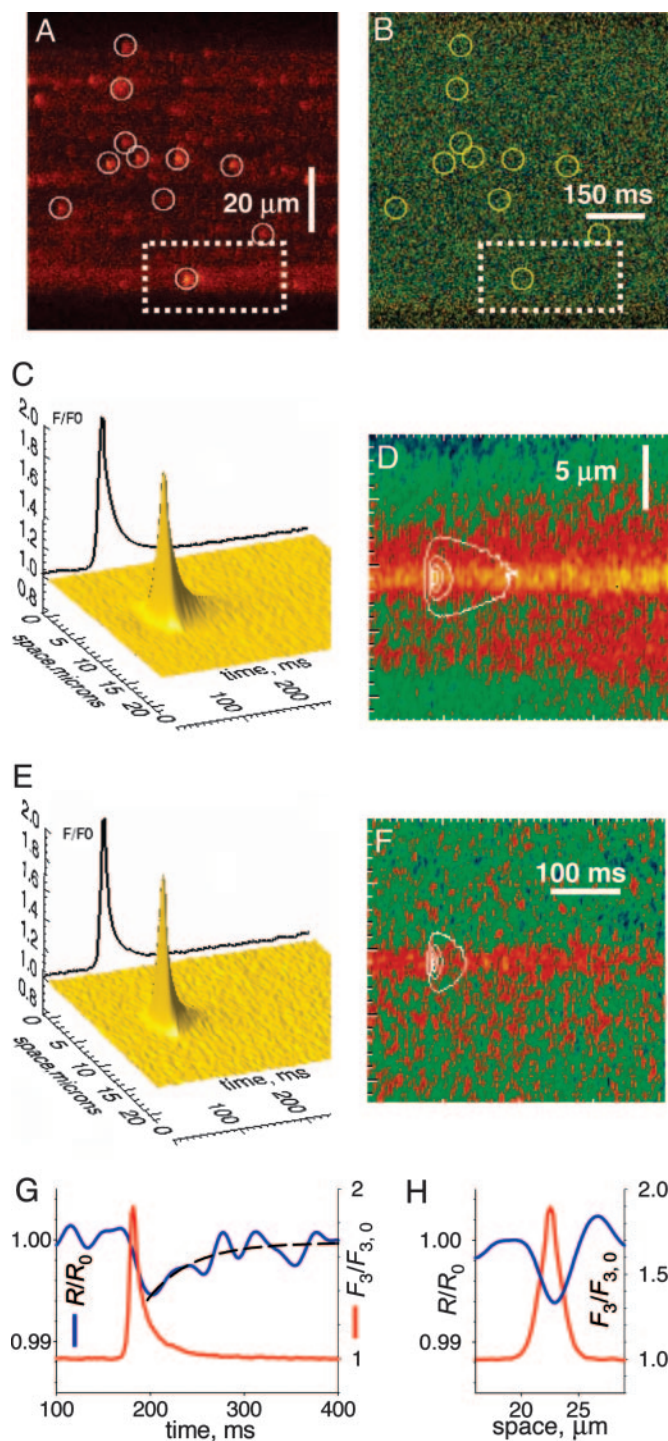


Fig. 1. Simultaneous imaging of cytosolic and intra-SR $[Ca^{2+}]$. (A) Line-scan $F_3(x, t)$ of rhod-2 in cytosol. Circles mark Ca^{2+} sparks. (B) SEER image $R(x, t) = F_1/F_2$ of mag-indo-1 in organelles. Circles repeated from A. (C) Average of subarrays (dashed rectangle in A) of F_3 around sparks. (D) Corresponding average of R , with spark overlaid. (E and F) Averages in cells with inhibited mitochondria. (G) Evolution of F_3 (red trace) and R (blue trace) at the spark center. The exponential fit (dashed trace) has an 0.56% amplitude and a τ of 48 ms. (H) Spatial profiles of F_3 at its peak (red trace) and R at nadir (blue trace).

is the average R image at the location of sparks in sulfate. The panel reveals a steady depression and a transient skrap (shown in Fig. 2 C–E) after normalization and filtering. In sulfate the nadir is deeper, reaching 1.5%, and the recovery time constant

is 251 ms. Differences in parameter values of the skrap in reference solution versus sulfate solution are entirely explained by the greater spark amplitude reached in sulfate (Fig. 7, which is published as supporting information on the PNAS web site).

The Delayed Onset of Skraps. The fractional change in ratio during skraps ranged from 0.006 (in reference solution) to 0.031 (in sulfate solution, in sparks of amplitude above the median), implying a reduction of $[Ca^{2+}]$ by at most 7.4%. A depletion of this magnitude is consistent with current estimates of Ca^{2+} current in a spark and Ca^{2+} content of the SR. By contrast, the kinetics of depletion were truly unexpected in that the phase of increasing depletion lasted too long. The flux of Ca^{2+} release underlying a spark (green trace in Fig. 2E) estimated by the rate of production of signal mass (14) was essentially over by the time the spark peaked. Surprisingly, $[Ca^{2+}]_{SR}$ continued to decrease afterward, reaching nadir 50 ms later.

Ca^{2+} Release Induced by Physiological Stimuli. The paradoxical kinetics of skraps is reflected in physiological cell-wide transients. Upon mechanical peeling, the transverse tubular system reseals, restoring electrical excitability (15, 16). Shown in Fig. 3A is the cytosolic Ca^{2+} transient in response to an action potential in a peeled fiber. Fig. 3B shows the simultaneously recorded SEER ratio, and Fig. 3C shows their averaged time courses, with release flux as a green trace. Upon Ca^{2+} release, $[Ca^{2+}]_{SR}$ fell from 980 to 900 μM , which is consistent with a depletion of $\approx 8\%$ of total SR Ca^{2+} and within the range of earlier estimates of fractional release caused by an action potential (10). As plotted in blue in Fig. 3A *Inset* and C, $[Ca^{2+}]_{SR}$ continued to decrease for 30 ms after cessation of release, repeating in the cell-wide signal the delay observed locally. The average delay was somewhat briefer than in sparks, perhaps because the action potential synchronizes not just the beginning but also the termination of sparks (17). Unlike skraps, cell-wide depletion did not visibly recover by 600 ms, which agrees with refilling times estimated by global photometry (18). The faster recovery of single skraps suggests that local depletion is replenished by diffusion from neighboring SR regions. The same hypothesis justifies that smaller skraps recover more rapidly.

A depletion delayed with respect to the flux that causes it violates conservation laws unless Ca^{2+} is released to the cytosol from a proximate source, distinct from the SR-luminal solution and therefore invisible to the monitoring dye. The evolution of $[Ca^{2+}]_{SR}$ upon stimulation of prolonged cell-wide Ca^{2+} release revealed other properties of this proximate store.

Ca^{2+} Transients Inside the Cellular Store. Fig. 4 shows successive xy scans in one fiber. Fig. 4A, rows a, shows images of F_3 (monitoring $[Ca^{2+}]$ in the cytosol, $[Ca^{2+}]_{cyto}$); in rows b are images of $[Ca^{2+}]_{SR}$. Fig. 4B shows image-averaged F_3 (red trace) and $[Ca^{2+}]_{SR}$ (blue trace). At the time indicated by the arrow in Fig. 4A, the solution was changed to a release-inducing (RI) solution, a low Ca^{2+} , low Mg^{2+} saline that induces moderate Ca^{2+} release. $[Ca^{2+}]_{cyto}$ increased, stayed elevated for tens of seconds, then decayed rapidly to resting values. Surprisingly, here and in 11 other cells, there was also a transient increase in $[Ca^{2+}]_{SR}$.

An analogous transient, described in suspensions of SR vesicles upon stimulation by RyR-opening drugs was traced to intravesicular Ca^{2+} release from CSQ (19). The intrastore buffer is clearly involved in the present transients as well. The flux, shown in green in Fig. 4B, exhibits two peaks corresponding to the two steps in the cytosolic Ca^{2+} transient. The first peak caused only a small reduction in $[Ca^{2+}]_{SR}$ (blue), which implies that the SR lumen was highly buffered. The second peak was essentially cotemporal with the $[Ca^{2+}]_{SR}$ peak and perhaps was driven by it. Afterward, release continued at a lower rate, but $[Ca^{2+}]_{SR}$ declined rapidly, reflecting a greatly reduced Ca^{2+}

Table 1. Properties of sparks and skrap

Condition	Skrap				Sparks				
	A	ttn, ms	W, μm	τ , ms	A	W, μm	RT, ms	n events	N cells
Reference	NA	NA	NA	NA	1.13	2.25	7.28	4,103	6
Inhibited	0.00	44	3.50	46.3	1.14	2.19	7.76	2,249	3
SO ₄	0.01	70	3.95	702	1.65	2.69	9.12	2,878	3
Inhibited	0.01	66	3.70	200	1.41	2.57	7.43	3,421	3
SO ₄ , all	0.01	68	3.85	251	1.52	2.68	8.21	6,299	6

For skrap, amplitude (A) and full width at half magnitude (W) are measured at nadir; for sparks, amplitude and full width at half magnitude are measured at peak. Both inhibited conditions are in the presence of mitochondrial inhibitors, with the first inhibited condition in reference and the second in SO₄. "SO₄, all" includes events in SO₄ and SO₄ inhibited. τ , time constant of recovery, RT, rise time; ttn, time to nadir; NA, not applicable.

buffering power. It follows that the initial surge in $[\text{Ca}^{2+}]_{\text{SR}}$ resulted from a decrease in buffering power, namely in the number or affinity of Ca^{2+} binding sites of the store buffer. This change is expected from CSQ, because this protein polymerizes and gains Ca^{2+} binding sites in the presence of elevated $[\text{Ca}^{2+}]$, whereas the opposite occurs as $[\text{Ca}^{2+}]$ is lowered (20).

In Fig. 5, the response to low Mg^{2+} consisted of two separate cytosolic waves propagating slowly from left to right in the images (Fig. 5A). Whereas the first wave of release into the cytosol at 7 s was accompanied by marked increase in $[\text{Ca}^{2+}]_{\text{SR}}$, the second wave, which occurred at 31 s with a largely depleted SR, resulted in immediate and marked reduction in $[\text{Ca}^{2+}]_{\text{SR}}$ (Fig. 5A Right and B Right). This observation and Figs. 8 and 9, which are published as

supporting information on the PNAS web site. establish a good SR Ca^{2+} load as a requisite for the intra-SR Ca^{2+} release.

Mitochondria contributed little to the signal and were iden-

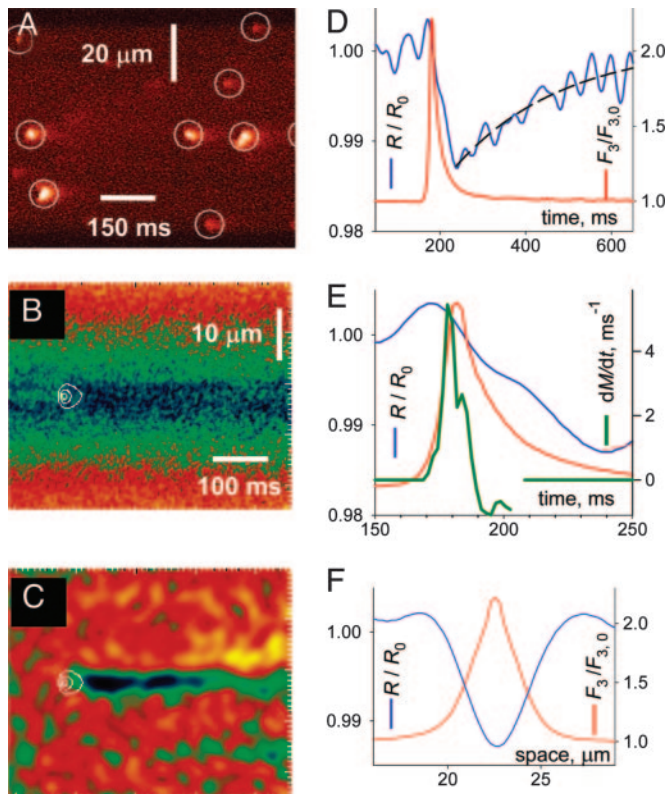


Fig. 2. Sparks and skrap enhanced by sulfate. (A) $F_3(x, t)$ in a fiber in sulfate. Note the larger sparks. (B) Average of spark regions in images R , located as in Fig. 1. (C) Image in B after low-pass filtering and normalization by prespark ratio, revealing a skrap. (D) Profiles at center of spark (red trace) or skrap (blue trace). The exponential fit (dashed trace) had an initial value of 1.5% and a τ of 251 ms. (E) Spark and skrap, with rate of signal mass production (dM/dt , green trace) as estimator of Ca^{2+} release flux. (F) Spatial profiles.

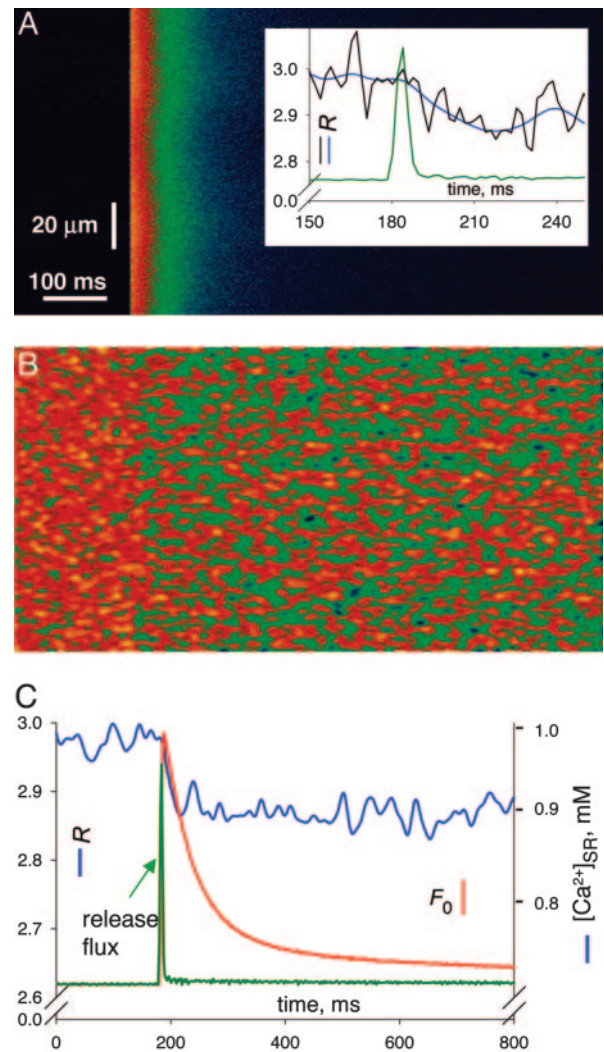


Fig. 3. SR depletion upon an action potential. (A and B) Averages of six line-scan images from a skinned frog fiber. (A) $F_3(x, t)$ normalized to its average before the stimulus. Inset shows profiles in expanded scale. The blue trace shows $R(t)$ from C. The black trace shows $R(t)$ calculated after minimal filtering to show the slow onset of depletion. (B) Average of corresponding R images. (C) profiles $F_3(t)$ (red trace) or $R(t)$ (blue trace) averaged over x . $[\text{Ca}^{2+}]$ scale calculated from equation 1 of ref. 11. The green trace shows the time course of release flux derived from F_3 in arbitrary units.

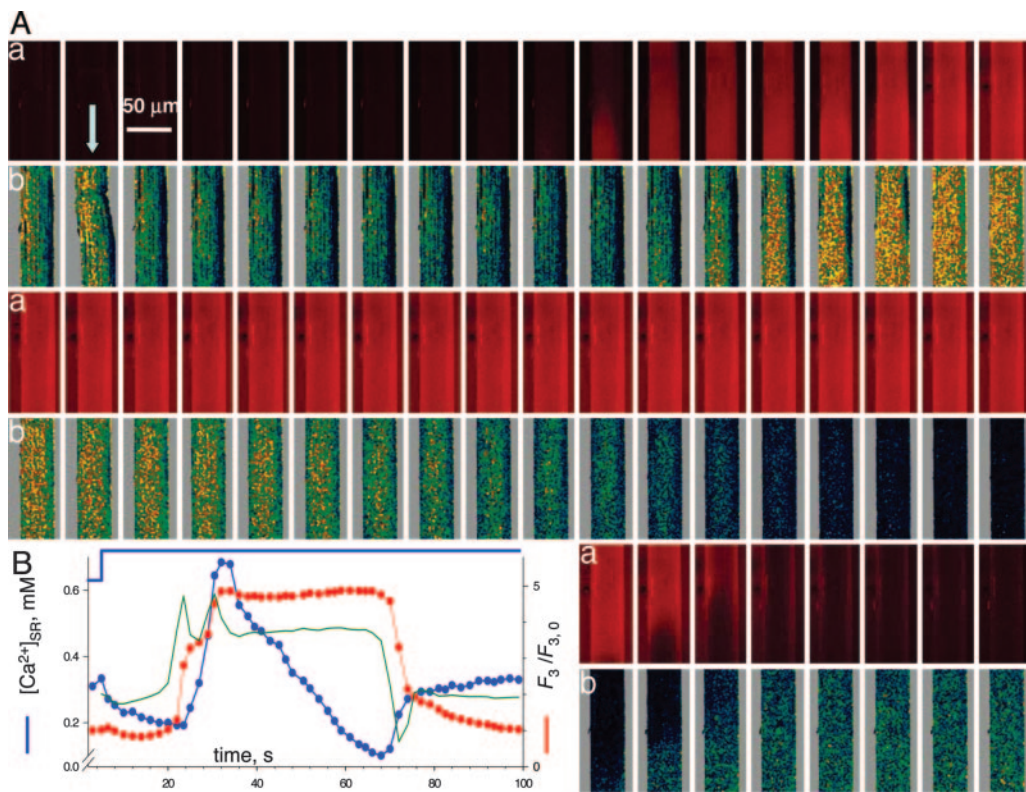


Fig. 4. Simultaneous imaging of cytosolic and SR $[Ca^{2+}]$. (A) Rows: a, xy scans of fluorescence F_3 of rhod-2; b, $[Ca^{2+}]_{SR}$ derived from images $R(x, y)$. (B) Image averages of $F_3/F_{3,0}$ (red trace) and $[Ca^{2+}]_{SR}$ (blue trace). During acquisition of the second set (arrow in A), the solution was changed to R1 solution (blue trace in B), eliciting Ca^{2+} release. An increase in $[Ca^{2+}]_{SR}$ followed shortly after the beginning of the cytosolic transient. The green trace shows the time course of Ca^{2+} release flux.

tified as regions of the image with initially low $[Ca^{2+}]$ (11), clearly visible in the $[Ca^{2+}]$ image at 5 s, Fig. 5B Left, and marked yellow in the binary mask of Fig. 5D. The evolution of the average R in mitochondrial areas (\bullet in Fig. 5E) features a

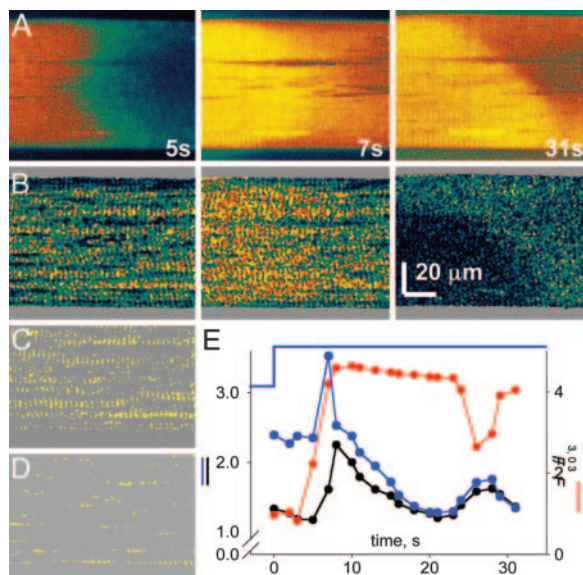


Fig. 5. $[Ca^{2+}]_{SR}$ during waves of Ca^{2+} release. (A) xy scans of fluorescence F_3 of rhod-2, selected from a series. (B) $[Ca^{2+}]_{SR}$ (x, y) derived from $R(x, y)$. (C) SR mask. Shown are areas where $R(x, y)$ before Ca^{2+} release was >2 . (D) Mitochondrial mask, where $R < 1.5$. (E) Average of F_3 (red trace) and R in SR mask (blue trace) or mitochondrial mask (black trace). The application of R1 solution is indicated at the top of the graph. (Scale bar: 20 μm .) Two waves of Ca^{2+} release move toward the right in A. The first wave in B Center is accompanied by increase in $[Ca^{2+}]_{SR}$. The second wave, instead, causes a sharp decrease in $[Ca^{2+}]_{SR}$.

transient in $[Ca^{2+}]$ that is minor and delayed by comparison with $[Ca^{2+}]_{SR}$. Fig. 9 shows that Ca^{2+} release in cells with poisoned mitochondria also resulted in a substantial $[Ca^{2+}]_{SR}$ transient.

Figs. 8–12 and *Supporting Text*, which are published as supporting information on the PNAS web site, illustrate other aspects of the increase in $[Ca^{2+}]_{SR}$. (i) The increase in $[Ca^{2+}]_{SR}$ occurred under a variety of triggers, including the signature RyR agonist, caffeine (Fig. 8), and sudden decreases in $[Ca^{2+}]_{cyto}$ (Fig. 10) (ruling out artifacts of the increase in $[Ca^{2+}]_{cyto}$); (ii) similar to the earlier observations with vesicular SR (19), the $[Ca^{2+}]_{SR}$ transient was most visible under moderate stimuli; (iii) increase in $[Ca^{2+}]_{SR}$ was often preceded by a brief decrease in $[Ca^{2+}]_{SR}$; and (iv) it could also be demonstrated by using the single- λ dye fluo-5N loaded inside the SR (Figs. 11 and 12), which rules out artifacts related to the chemistry of one particular dye.

Discussion

A Proximate Ca^{2+} Store. Both the delayed onset of depletion in skrapas and the $[Ca^{2+}]_{SR}$ transient observed during prolonged cell-wide Ca^{2+} release appear to violate the laws of mass conservation. Both observations are explained if the SR buffer provides a kinetically distinct Ca^{2+} compartment, which must be proximate (topologically close to the release channels), so that it constitutes the immediate source for release during a spark. The delayed depletion is then explained as flux from the SR lumen to reload Ca^{2+} lost from the buffer during a spark. Our work offers no evidence for a specific chemical nature of this compartment, which therefore remains purely hypothetical. However, known properties of CSQ are intriguingly consistent with the biophysical features required to explain the present results.

In terminal cisternae of skeletal muscle, CSQ forms linear polymers, visible as a fibrillar network (21). Bonds with triadin and junctin (22) place CSQ polymers near the luminal mouth of RyRs. Ca^{2+} favors formation of these polymers and stabilizes

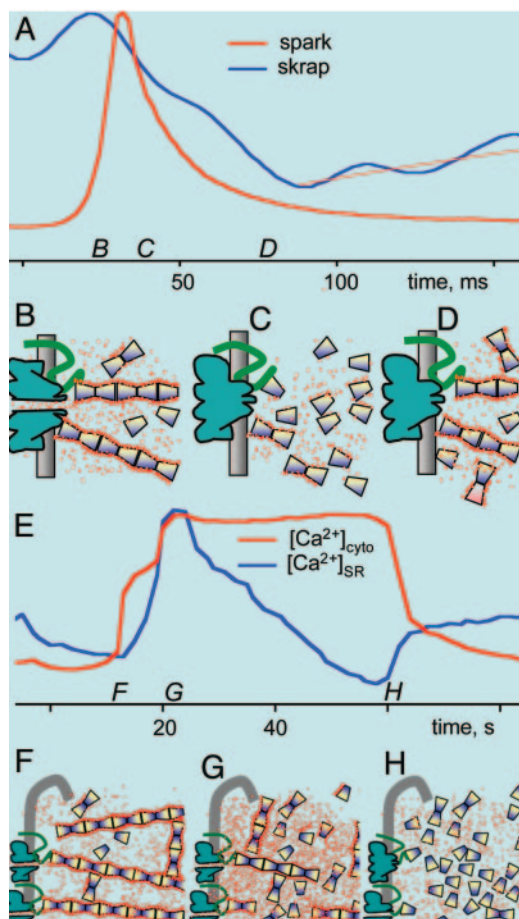


Fig. 6. A proximate source of releasable Ca^{2+} . A proposal to reconcile the paradoxical evolution of $[\text{Ca}^{2+}]_{\text{SR}}$ with features of the main store buffer, demonstrated in ref. 20 for CSQ in aqueous solutions. (A) Spark and skrap from 2E. (B–D) Putative states of the proximate store at times B–D. (B) The channel opens, and Ca^{2+} adsorbed to linear CSQ polymers feeds rapid release. (C) At time C the polymers are depleted and, hence, disassemble, a conformational change that could be transmitted by triadin as a signal for channel closure. (D) Depletion becomes deeper as Ca^{2+} replenishes the proximate store and the CSQ polymer reassembles. (E) $[\text{Ca}^{2+}]_{\text{cyto}}$ and $[\text{Ca}^{2+}]_{\text{SR}}$ during prolonged release, from Fig. 4B. (F) At resting, $[\text{Ca}^{2+}]_{\text{SR}}$ CSQ polymers provide maximum Ca^{2+} binding. At time F, release lowers local $[\text{Ca}^{2+}]_{\text{SR}}$. (G) The polymer disassembles, and Ca^{2+} dissociates, causing the intra-SR transient. (H) As Ca^{2+} release continues, CSQ depolymerizes fully.

them, occupying a layer where it is adsorbed rather than bound (20). In this layer, Ca^{2+} is able to diffuse laterally and should be readily deliverable to the open channels (20). According to the properties of CSQ in aqueous solutions, this polymer-specific bound Ca^{2+} could constitute the proximate store, evolving as illustrated in Fig. 6: the rising phase of a spark (at time B in Fig. 6A) is due to Ca^{2+} release from CSQ polymers (Fig. 6B); this delivery should cause depolymerization, i.e., disassembly of the proximate store (Fig. 6C); continuing depletion afterward would reflect repolymerization and refilling of the proximate store (Fig. 6D).

The $[\text{Ca}^{2+}]_{\text{SR}}$ transient during prolonged cell-wide release, reproduced in Fig. 6E, is explained likewise: Fig. 6F represents the resting situation (at times F in Fig. 6E). In the well loaded SR, CSQ is polymerized (20). During Ca^{2+} release, $[\text{Ca}^{2+}]_{\text{SR}}$ will decrease near release sites, which should cause widespread depolymerization of CSQ (20) with loss of binding sites (20) and release of Ca^{2+} to the SR lumen (Fig. 6G). Ca^{2+} release afterward will find a less buffered SR, resulting in rapid decay in

$[\text{Ca}^{2+}]_{\text{SR}}$ and further depolymerization of CSQ (Fig. 6H). Whether a net increase in $[\text{Ca}^{2+}]_{\text{SR}}$ is observed will depend on the balance between exit rate of Ca^{2+} from CSQ and flux through release channels. From the present observations it appears that twitches in response to isolated action potentials only result in reduction of $[\text{Ca}^{2+}]_{\text{SR}}$, whereas increases in $[\text{Ca}^{2+}]_{\text{SR}}$ require more prolonged stimulation of Ca^{2+} release.

Advantages of a Dynamic Store. In 1968, Adam and Delbruck (23) proposed that ligand binding to cell surface receptors is enhanced by the two-dimensional diffusion that follows membrane adsorption of the ligands. This so-called reduction of dimensionality increases efficiency of diffusion (24) by a factor that may reach hundreds (25). The “perfect sink” version of this theory (26) applies to delivery of ions to an open channel. Because CSQ polymers are linear structures, of one dimension, adsorption to them would involve further reduction of dimensionality and diffusion enhancement. Given this dimensional advantage, CSQ polymers would function as “calcium wires,” which efficiently deliver Ca^{2+} to the channel mouth (20).

As we have found, depletion of the SR lumen is small, probably too small to convey the robust signal that closes channels to terminate sparks. This conclusion is especially obvious considering that depletion is only starting to develop at the time the channels close, at the peak of the spark (Fig. 6A). However, depletion of the proximate store could mediate channel gating. Indeed, CSQ depolymerizes upon loss of bound Ca^{2+} . This structural change could have gating effects via triadin or junctin, as represented in Fig. 6C by an altered triadin and a closed channel. In this view, the proximate store would not just improve delivery of Ca^{2+} but also signal the channel to close after a set number of ions are delivered to it. Such an “ion-counting” device (first contemplated under different assumptions in ref. 27) should be especially useful with Ca^{2+} , an ion with multiple signaling functions.

Finally, we have seen that under appropriate, albeit artificial, stimuli, the SR buffer may release bound Ca^{2+} and cause a transient inside the SR. In the examples, these transients helped sustain the $[\text{Ca}^{2+}]$ gradient that drives flux, thus delaying the effects of depletion under prolonged Ca^{2+} release. Ca^{2+} signaling is thought to be the role of membrane channels in cells and organelles (28). The intrastore Ca^{2+} transients demonstrated here suggest a different strategy, control of the driving force for Ca^{2+} release through changes in conformation or the aggregation state of cellular buffers. Combined with the targeted delivery of Ca^{2+} by linear polymers, local control of store $[\text{Ca}^{2+}]$ by buffer aggregation could contribute to the specificity of the signals over wide-ranging scales of time, space, and Ca^{2+} concentration.

Methods

Single semitendinosus muscle fibers of *Rana pipiens* were imaged. Frogs were decapitated under anesthesia, a procedure approved by Rush University’s Institutional Animal Care and Use Committee. Muscles were incubated for 120 min at 18°C in Ringer’s solution with 10 μM mag-indo-1 acetoxyethyl (AM). Fiber segments were mounted, stretched under pins, and membrane-permeabilized with 0.002% saponin (29) or mechanically skinned before mounting.

Solutions. For permeabilized cells, the reference solution contained (in mM): 70.6 mM K glutamate, 5 mM Na_2ATP , 10.29 mM Na_2 creatine phosphate, 1 mM EGTA, 5 mM glucose, 10 mM Hepes, 1 mM caffeine, 8% dextran, 25 μM *n*-benzyl-*p*-toluene sulfonamide (BTS; Sigma-Aldrich), 100 μM rhod-2, 0.186 mM CaCl_2 , and 4.96 mM MgCl_2 for a nominal $[\text{Ca}^{2+}]$ of 100 nM and $[\text{Mg}^{2+}]$ of 0.4 mM. Sulfate solution had 74.5 mM K_2SO_4 instead of glutamate, no caffeine, 5.5 mM MgCl_2 , and

